THE JOURNAL OF THE ACOUSTICAL SOCIETY OF KOREA VOL.25, NO.3E 2006. 9 pp. 131~135

The Perfectly Matched Layer applied to the Split-Step Padé PE Solver in an Ocean Waveguide

Keunhwa Lee*, Woojae Seong*
*Dept. of Naval Architecture and Ocean Engineering, Seoul National University, Seoul, KOREA
(Received September 21 2006; accepted October 10 2006)

Abstract

The PML developed for the radio wave propagation is a powerful numerical domain truncation technique. We perform an analytic study on the reflection from the PML inserted in the ocean bottom. In the ocean bottom, we show the PML to have the improved performance but simultaneously the degeneration below the critical angle of the fast ocean bottom. The degeneration of the PML can be simply relaxed by stretching the thickness of the PML or putting the attenuation coefficient to the ocean bottom. As a better solution, we propose the improved truncation technique based on the PML and the non-local boundary condition. Finally, we apply the PML to the acoustic wave propagation using split-step Padé PE solver. For the problems of the ocean waveguide, the numerical efficiency of the PML is examined and the usefulness of the PML is confirmed.

Keywords: *Perfectly matched layer, Non-local boundary condition, Reflection analysis, Ocean bottom, Split-step Padé PE.*

I. Introduction

The Perfectly matched layer (PML) has been introduced by Berenger [1] as an absorbing boundary condition (ABC) for the electromagnetic waves. The PML theoretically exhibits the zero reflection at the interface between the free space and PML for all frequencies and all grazing angles [2]. But, when performing the numerical calculation, the PML cannot avoid the artificial reflection resulting from two causes. One is the reflection caused by the finiteness of the numerical domain and the other is the discretization-induced reflection. For many physical problems, these unwanted reflections can be reduced to an insignificant level by the proper choice of the PML coefficient and thickness. In order to act as an excellent absorber, the PML only need to be the thickness of 10~40 grid points [3-6].

In spite of the efficiency of the PML, the PML has not been usually recommended as the ABC for the long range propagation problem [6]. This is because the PML is degenerated as the direction of the propagation wave is close to the low grazing angle region [5-8]. In that case, the magnitude of the artificial reflection has the value close to 1 and the PML fails to absorb the wave energy. But, the above statement for the degeneration of the PML isn't clear for the PML inserted to the ocean bottom. Since the ocean bottom plays the role of filtering the high grazing angle rays, the waves transmitted from the ocean bottom to the PML may be the propagation waves or the evanescent waves [9]. This twofold behavior of the acoustic wave can affect the efficiency of the PML, different from that of the free space PML. Therefore, the general performance study is required for the PML inserted in the ocean bottom.

In this paper, we analytically study the reflection from the PML inserted in the ocean bottom. The role of the ocean bottom on the PML performance is examined. Especially, we propose the improved truncation techniques based on the PML and the non-local boundary condition (NLBC) [10-12]. Finally, the PML is applied to SNUPE (Seoul National University Parabolic Equation), the stability improved split-step Padé PE solver [13]. For ocean waveguide problems, the numerical proof of the PML is performed.

Corresponding author: Keunhwa Lee (nasalkh2@snu.ac.kr)
Dept. of Naval Architecture and Ocean Engineering, Seoul National University, Seoul, 151-744 Korea

II. Reflection from the Ocean Bottom Plus PML

In the 2D coordinate (r,z) for the parabolic equation, the PML can be expressed in terms of the complex coordinate-stretching variables z^* as

$$z^* = z + \frac{j}{\omega}\int_0^z \sigma(z')dz' \tag{1}$$

where ω is the angular frequency and $\sigma(z')$ is the depth-varying PML coefficient.

The reflection coefficient between the free space and the PML with a finite thickness and the pressure release condition at the lower boundary of the PML is presented as

$$R = -e^{j2k_1\delta}e^{-\frac{2k_1}{\omega}\int_0^\delta \sigma(z')dz'} \tag{2}$$

with the PML thickness of δ. Here, the vertical wavenumber $k_1 = k\sin\theta$ with the grazing angle θ and the medium wavenumber k [5].

Equation (2) is itself the artificial reflection. The first term of equation (2) is for the phase shift and the second term represents the attenuation by the PML. The minus sign is caused by the pressure release boundary condition. Specifically, we observe that the reflection coefficient is close to 1 when $\theta \to 0$.

Assuming the environment of Fig. 1 and the plane wave, the total reflection from the general ocean bottom is derived as below.

$$R_0 = \frac{R_{00} + R_1 e^{j2k_1 h}}{1 + R_{00}R_1 e^{j2k_1 h}} \tag{3}$$

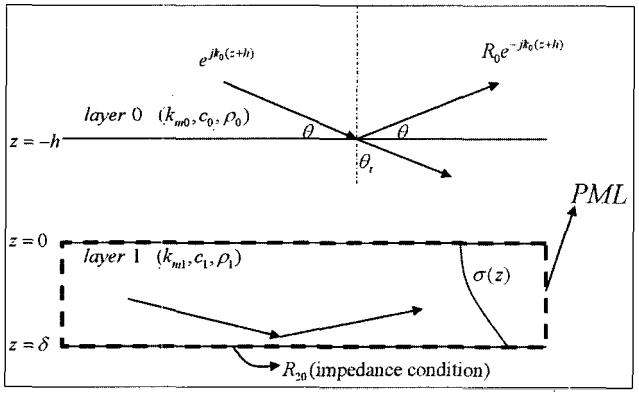

Fig. 1. Schematic diagram of the PML inserted to the simple two ocean bottom.

where $R_{00} = \frac{k_0/\rho_0 - k_1/\rho_1}{k_0/\rho_0 + k_1/\rho_1}$ with the vertical wavenumber $k_i (i = 0, 1,\ i$ is layer index) and the density ρ_i and $R_1 = R_{20}e^{j2k_1\delta}e^{-\frac{2k_1}{\omega}\int_0^\delta \sigma(z')dz'}$ with the local reflection coefficient R_{20} at $z = \delta$. R_{20} is assumed as a known parameter. And, $\phi_i(z^-) = \phi_{i+1}(z^+)$ and $\frac{1}{\rho_i}\frac{\partial\phi_i}{\partial z^*}\Big|_{z=z^-} = \frac{1}{\rho_{i+1}}\frac{\partial\phi_{i+1}}{\partial z^*}\Big|_{z=z^+}$ are used as the continuity relation between layers. Here, $\phi_i(z)$ means the wave potential.

If the numerical domain is infinite and the PML is absent, the true reflection from the ocean bottom is R_{00}. Thus, the artificial reflection is derived as difference of the equation (2) and R_{00} as below.

$$\Delta R = R_0 - R_{00} = \frac{4k_0k_1R_1e^{j2k_1h}/\rho_0\rho_1}{(k_0/\rho_0 + k_1/\rho_1)^2(1 + R_{00}R_1e^{j2k_1h})} \tag{4}$$

where the vertical wavenumber $k_i = \sqrt{k_{mi}^2 - (k_{m0}\cos\theta)^2} = \frac{\omega}{c_i}\sqrt{1-(\frac{c_i}{c_0})^2\cos^2\theta}$ with the sound speed c_i and the medium wavenumber k_{mi}.

Equation (4) can explain the effect of the acoustic wave filtered by the ocean bottom. In underwater acoustics, equation (4) is more appropriate than equation (2) since it reflects the real ocean environment.

In equation (4), when $\theta \to 0$, $\Delta R \to 0$. This is caused by the behavior of k_0. Physically, the acoustic waves propagated at the low grazing angle are intercepted by the ocean bottom and the wave energy can hardly transmit in the ocean bottom. As a result, the PML with the ocean bottom shows the improved performance in the low grazing angle region. But, this statement isn't true for the fast ocean bottom. For the fast ocean bottom, the acoustic wave below the critical angle becomes evanescent waves and $R_1e^{j2k_1h}$ of equation (4) is expressed as

$$R_1e^{j2k_1h} = R_{20}e^{j2k_1(\delta+h)}e^{-\frac{2k_1}{\omega}\int_0^\delta \sigma(z')dz'} = R_{20}e^{-2\gamma_1(\delta+h)}e^{-j\frac{2\gamma_1}{\omega}\int_0^\delta \sigma(z')dz'} \tag{5}$$

where $\gamma_1 = \frac{\omega}{c_1}\sqrt{(\frac{c_1}{c_0})^2\cos^2\theta - 1}$.

In evanescent region, the property of two exponential terms of $R_1e^{j2k_1h}$ is respectively exchanged as the upper equation. Since the attenuation term of the PML is changed to the phase term, the effect of the PML naturally disappears. Instead, the first exponential term of equation (5) behaves like the new absorber. Although this new absorber may show excellent performance as

the grazing angle becomes lower and $(\delta+h)$ and c_1/c_0 is larger, the total ability of the ABC is degenerated when compared to that of the PML. Especially, the worst degeneration happens in the critical angle. When γ_1 is zero, the artificial reflection becomes -2 where the total reflection is -1 and the true reflection is 1. In this case, all exponential terms of equation (5) becomes close to 1 and lose the ability of the absorber perfectly. Undoubtedly, the degeneration of the low grazing angle region cancels out each other when $(\delta+h)$ or c_1/c_0 is larger. But, it is inevitable that the singular error happens in the critical angle.

III. Improved Performance of the PML in the Ocean Bottom

The degeneration of the PML for the fast ocean bottom can be simply compensated by stretching the thickness $(\delta+h)$ or putting the attenuation factor for the ocean bottom.

In Fig. 2, we plot the behavior of the reflection as the thickness increases. To simplify the problem, h is assumed to the zero and the variation by only the δ will be observed. R_{20} is set to -1, the pressure-release condition. The sound speed of the layer 0 is $1500\,m/s$ and that of layer 1 is $1600\,m/s$. The density is set to $1000\,kg/m^3$ for all layers. The thickness δ is considered as multiples of the wavelength and $\delta = nc_2/f = n\lambda\ (n=1,2,3,4)$ for the example of Fig. 2. The PML coefficient is $\sigma(z)=\sigma_m(\frac{z}{\delta})^2$ and $\sigma_m=\frac{3c_2}{2\delta}\alpha$ where α is the arbitrary positive number [5]. To suppress the discretization-induced reflection, we make $\sigma_m\cdot\Delta z$ have the magnitude order smaller than $O(10^3)$ where $\Delta z \approx \lambda/15$ for all examples [7].

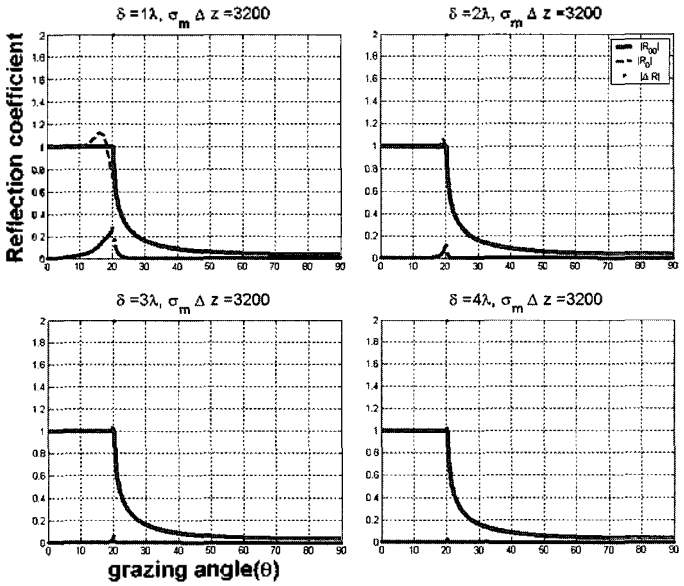

Fig. 2. The effect of the thickness δ of the on the artificial reflection (*solid line*: true reflection coefficient, dash line: total reflection coefficient, dotted line: artificial reflection coefficient).

In Fig. 2, in spite of being a fast ocean bottom, we observe that the artificial reflection is reduced as the thickness increases. And the approximately zero reflections for all angles is obtained with the thickness over 3λ although the constant singular error exists in the critical angle. We emphasize that the zero reflection has never been obtained with the traditional ABCs for same case [4][12].

As a second example, we show the improved performance by putting attenuation in the ocean bottom. The values used in the second example are same as the first example except fixing the thickness to 3λ. If the attenuation exists in layer 1, the transmitted angle θ_t is always a complex number. We consider $\theta_t=\theta_0+j\theta_1$ where θ_0 and θ_1 are real. Then, the vertical wavenumber k_1 of layer 1 can be approximately transposed to $k_{m1}(\frac{\varepsilon}{\sinh\theta_1}+j\sinh\theta_1)$ with the attenuation factor ε in the evanescent region. Using this relation, R_1 is arranged as

$$R_1 \approx -e^{j2k_{m1}(\frac{\delta c}{\sinh\theta_1}\frac{\sinh\theta_1}{\omega}\int_0^{\delta}\sigma(z')dz')}\; e^{-2k_{m1}(\delta\sinh\theta_1+\frac{\varepsilon}{\omega\sinh\theta_1}\int_0^{\delta}\sigma(z')dz')} \qquad (6)$$

Equation (6) explains the effect of the attenuation factor. Although $\theta_1\to 0+0j$ in the critical angle, the exponential term for the attenuation still remains and approach to a small number.

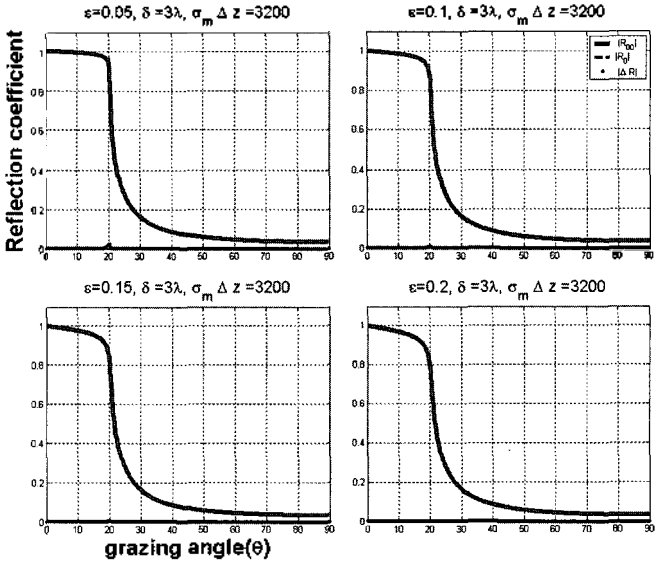

Fig. 3. The effect of the attenuation factor on the artificial reflection (solid line: true reflection coefficient, dash line: total reflection coefficient, dotted line: artificial reflection coefficient). The ε described in the plot has the dimension of dB/λ.

So, we know that the attenuation factor suppresses the sudden degeneration of the ability of the absorber near the critical angle for the fast ocean bottom. In Fig. 3, we observe the singular error near the critical angle to be much smaller than in Fig. 2. The singular error in the critical angle is also reduced.

Finally, we will show the effect of the lower boundary of the PML expressed as R_{20}. If we impose the low-order NLBC (Standard PE) to the lower boundary of the PML, R_{20} is expressed in the frequency-wavenumber domain as below [11].

$$R_{20} = \frac{\sqrt{1+\cos\theta_t} - \sqrt{2}}{\sqrt{1+\cos\theta_t} + \sqrt{2}} \tag{7}$$

Then, R_1 is rearranged as

$$R_1 = R_{20} e^{j2k_{m1}\sin\theta_t \delta} e^{-\frac{2k_{m1}\sin\theta_t}{\omega}\int_0^{\delta}\sigma(z')dz'} = \frac{\sqrt{1+\cos\theta_t} - \sqrt{2}}{\sqrt{1+\cos\theta_t} + \sqrt{2}} e^{j2k_{m1}\sin\theta_t \delta} e^{-\frac{2k_{m1}\sin\theta_t}{\omega}\int_{\delta}^{\delta}\sigma(z')dz'} \tag{8}$$

In equation (8), we can easily confirm $R_1 \to 0$ when $\theta_t \to 0 + 0j$. Although $\theta_t \to 0 + \varepsilon j$, $R_{20} \approx 0$ and $R_1 \to 0$ since ε is usually a small number less than 1 in the ocean environment. Although we use the lower-order PE operator to the lower boundary condition, the artificial reflection in evanescent region is almost perfectly eliminated. This interesting result indicates that more powerful truncation technique for all angles is made by the combination of the PML and the low-order NLBC. Naturally, the additional numerical cost will be required to calculate the low order NLBC at the expense of the combination. In Fig. 4, we plot the reflection considering the NLBC. All values used in this example are equal to that of the first example except the use of the NLBC. As shown in Fig. 4, the maximum value of the artificial reflection has the order of $O(10^{-4})$. The artificial reflection in the low grazing angle region is reduced more as the thickness increases and in the high grazing angle region is reduced more as the PML coefficient increases. In the critical angle, the artificial reflection is always zero because of the low-order NLBC.

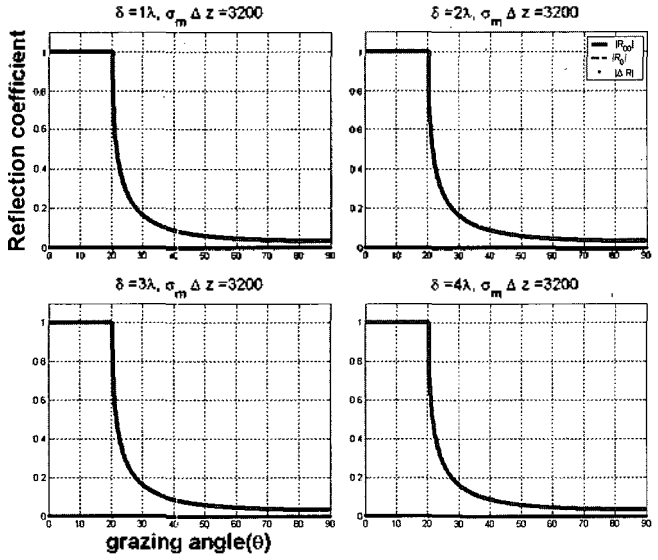

Fig. 4. The effect of the low-order NLBC (SPE) on the artificial reflection (solid line: true reflection coefficient, dash line: total reflection coefficient, dotted line: artificial reflection coefficient).

IV. Numerical Modeling Using PE Solver

The acoustic parabolic equation applied to the PML is formulated as below.

$$\frac{\partial p}{\partial r} = ik_0\left[-1 + \sqrt{n^2(z) + \frac{1}{k_0^2}\frac{\rho}{(1+j\sigma(z)/\omega)}\frac{\partial}{\partial z}\left(\frac{1}{\rho(1+j\sigma(z)/\omega)}\frac{\partial}{\partial z}\right)}\right]p \tag{9}$$

We solve equation (9) using the routine of SNUPE [13].

V. Numerical Examples

We will show two numerical examples in this section. First example is Lloyd mirror problem. The frequency is 50Hz and the source is located on the depth of 36m. The ocean sound speed and density are $1500m/s$ and $1000kg/m^3$. These acoustic properties are used for all examples. Fig. 5 shows the result for Lloyd mirror problem. Although the PML thickness increases from $\delta = \lambda$ to $\delta = 4\lambda$, the numerical solution doesn't converge

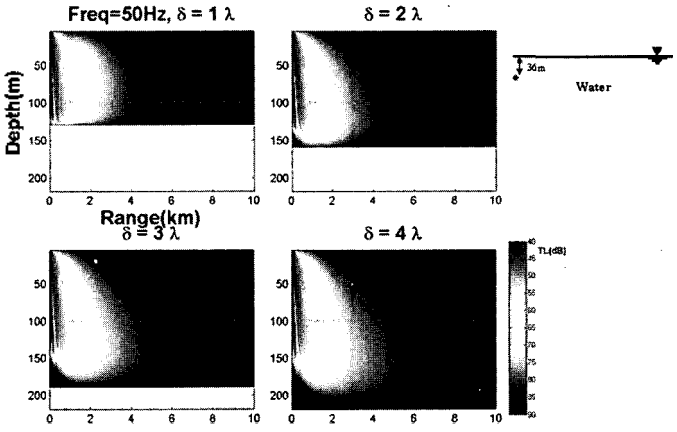

Fig. 5. Lloyd mirror problem: the transmission loss for the PML thickness. The dotted line indicates the interface between the real numerical domain and the PML.

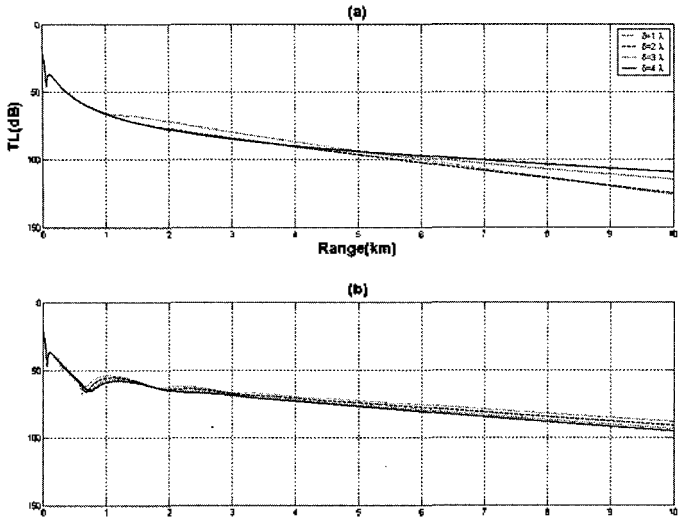

Fig. 6. Transmission loss for Lloyd mirror problem at the depth of 36m for the thickness of the absorbing layer. (a) PML, (b) Traditional absorbing layer.

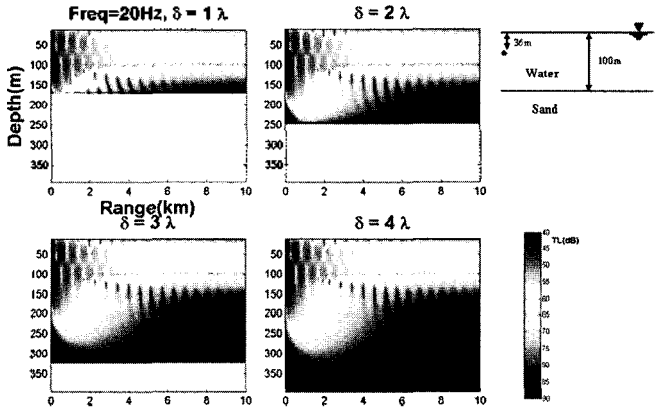

Fig. 7. Pekeris waveguide: the transmission loss for the PML thickness. The dotted line indicates the interface between the real numerical domain and the PML.

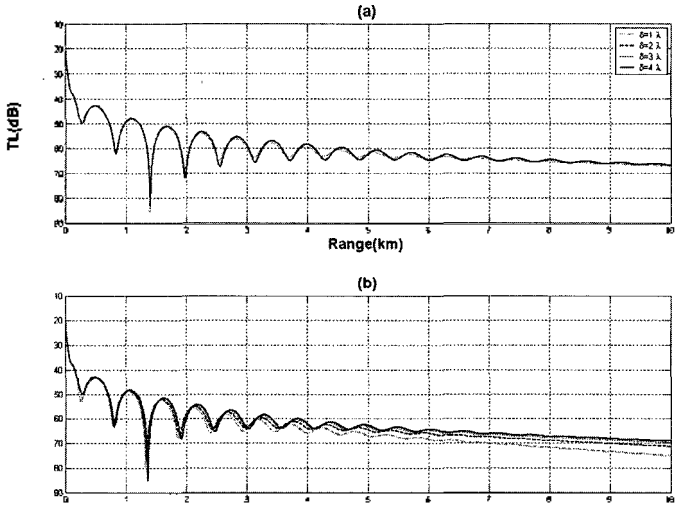

Fig. 8. Transmission loss for Pekeris waveguide at the depth of 36m for the thickness of the absorbing layer. (a) PML, (b) Traditional absorbing layer.

in the long range. Fig. 6 (a) shows the transmission loss at the source depth for the PML thickness. The solution cannot be stable. This is because the PML is naturally degenerated in the long range of the free field space. This degeneration is estimated from the equation (2). Fig. 6(b) is plotted to compare the results of the PML and the traditional absorbing layer (TAL). The thickness of the TAL is set equal to that of the PML and the absorbing coefficient is varying from $0.0dB/\lambda$ to $10.0dB/\lambda$ for the thickness of the absorbing layer. For the long range, the result of the TAL describes more stable than that of the PML but the solution is still inaccurate.

In Second example, Pekeris environment is considered in order to show the improved performance of the PML in ocean bottom. The ocean depth is 100m and the source depth is equal to that of first example. Bottom sound speed, bottom density and attenuation is respectively $1800m/s$, $1800kg/m^3$ and $0.5dB/\lambda$. The source frequency is 20Hz. In Fig. 7, we observe the wave field is converged even to $\delta = 2\lambda$. This is totally because of the role of the ocean bottom and its attenuation. The performances of the PML and the TAL are compared in Fig. 8, showing the transmission loss at the source depth. We can see that the PML is superior to the TAL.

VI. Summary

In order to apply the PML to the parabolic equation in an ocean waveguide, we perform the reflection analysis for the PML included in the ocean bottom. New analytic reflection coefficient is derived and the efficiency of the PML is examined for the ocean bottom. The PML obtains some gain for the soft ocean bottom but is degenerated below the critical angle for the fast ocean bottom. We show that this degeneration is resolved by stretching the thickness of the layer, putting the attenuation factor or using the low-order NLBC. Finally, we apply the PML to the split-step Padé parabolic solver and validate the efficiency of the PML in the ocean bottom through two examples.

References

1. J. P. Berenger, "A perfectly matched layer for the absorption of electromagnetic waves," J. Comput. Phys., 114, 185-200 (1994)
2. W. C. Chew and Q. H. Liu, "Perfectly matched layers for elastodynamics: a new absorbing boundary condition," J. Comp. Acoust., 4, 72-79 (1996)

3. E. Turkel and A. Yefet, "Absorbing PML boundary layers for wave-like equations," Appl. Numer. Math., 27, 533-557 (1998)
4. F. Q. Hu, "Absorbing boundary conditions," Int'l. J. Comput. Fluid D., 18, 513-522 (2004)
5. F. Collino, "Perfectly matched absorbing layers for the paraxial equations," J. Comput. Phys., 131, 164-180 (1997)
6. M. Levy, Parabolic equation methods for electromagnetic wave propagation (IEE, LONDON, 2000)
7. D. T. Prescott, "Reflection analysis of FDTD boundary conditions-part II: Berenger's PML absorbing layers," IEEE Trans. Microwave Theory Tech., 45, 1171-1178 (1997)
8. D. Yevick and D. J. Thomson, "Impedance-matched absorbers for finite-parabolic equation algorithms," J. Acoust. Soc. Am., 107, 1226-1234 (2000)
9. H. Medwin and C. S. Clay, Fundamentals of acoustical oceanography (ACADEMIC PRESS, Boston, 1998)
10. G. H. Brooke and D. J. Thomson, "Non-local boundary conditions for high-order parabolic equation algorithms," Wave Motion, 31, 117-129 (2000)
11. K. Lee and W. Seong, "Analytic error caused by the inconsistency of the approximation order between the non-local boundary condition and the parabolic governing equation," J. Acoust. Soc. Kr., 25, 229-238 (2006)
12. D. Givoli, Numerical methods for problems in infinite domains (ELSEVIER, New York, 1992)
13. T. Kim and W. Seong, "Stability improved split-step parabolic equation model," J. Acoust. Soc. Kr., 21, 105-111 (2003)

[Profile]

•Keunhwa Lee
2000, B.S. in Naval Architecture & Ocean Eng., Seoul Nat'l Univ.
2006, Ph.D. in Naval Architecture & Ocean Eng., Seoul Nat'l Univ.
2006-preset, BK21 Post-doctoral Researcher, Marine Technology Education and Research Center, Seoul Nat'l Univ.
※ Areas of interest: Ocean/Sediment interaction problem, Taget and diffuse scattering modeling, Inverse problem of the acoustic measurement.

•Woojae Seong
1982, B.S. in Naval Architecture & Ocean Eng., Seoul Nat'l Univ.
1990, Ph.D. in Ocean Engineering, MIT
1991, MIT Post-dotorial associate
1992-1996, Professor in Ships and Ocean Eng., Inha Univ.
1996-present, Professor in Naval Architecture & Ocean Eng., Seoul Nat'l Univ.
※ Areas of interest: Propagation modeling, Geo-acoustic inversion, Matched field processing, Acoustic monitoring, Sonar applications for AUV.